

CFD Modeling of the Flow Around a Ducted Tip Hydrofoil

Hildur Ingvarsdottir¹
Dr. Carl Ollivier-Gooch¹
Dr. Sheldon I. Green¹

The flow over a finite-span hydrofoil has been studied using the finite-volume flow solver CFD-ACE(U) from CFD Research Corporation. The aim of the study was to provide a good basis for future modeling of ducted tip hydrofoils and a ducted tip propeller. A $k-\epsilon$ turbulence model and a combination of C-H, H-H and prismatic grids were used to cover the flow domain. Cases were run with a second order accurate upwind differencing scheme using approximately 150,000 – 436,000 cells. Comparison with experimental data showed that away from the tip of the hydrofoil the pressure distribution was well predicted and sectional lift was predicted within 2% of experimental data whereas closer to the tip the difference in lift reached up to 12%. The total lift is in good agreement with lifting line theory. It was also shown that the spanwise location of the vortex core was well predicted. Future work will include developing a solid model of a hydrofoil with a ducted tip and running simulations for the flow around it. A final stage of the research will involve simulation and optimization of ducted tip propellers.

INTRODUCTION

All lifting surfaces that terminate in a moving fluid create tip vortices. Tip vortices on marine propellers have two undesirable effects: they reduce the efficiency of the blade and they may cause tip vortex cavitation. The latter typically occurs well before blade and hub cavitation. Cavitation is an undesirable effect since it can cause pitting and erosion of the propeller and surrounding equipment and is also a source of vibration and noise.

There are several devices that have been tried or are being used to reduce the effects of tip vortices. The most commonly used means is the Kort nozzle. The Kort nozzle has the form of a shaped duct that fits with a fairly small clearance around the propeller. Kort nozzles can improve the efficiency of highly loaded propellers by up to 10 percent but the added wetted surface creates extra drag, which implies a reduction in efficiency when the propeller is less heavily loaded (Hordnes and Green, 1998). Other devices that have been proposed to alleviate the effects of tip vortices include bulbous tips installed on propeller blades (Crump, 1948), porous blade tips (Mani et al., 1988) and fitting small bladelets to each propeller blade tip (Itoh et al., 1987).

A number of computational studies have been done on tip vortices, both in aerodynamic and marine applications. Two studies of the most relevance to the current work were done by Hsiao and Pauley (1998) and Dacles-Mariani et al. (1995). Hsiao and Pauley conducted a numerical study of the steady state tip vortex flow over a finite-span hydrofoil. They studied the effects of angle of attack, Reynolds number and the hydrofoil planform on the tip vortex. After obtaining a good agreement between the numerical pressure distribution along the hydrofoil and experimental data, they studied the roll-up of the tip vortex. Dacles-Mariani et al. (1995) carried out interactively a computational and experimental study of the wingtip vortex in the near field. They applied inflow and outflow boundary conditions from the experimental data and obtained good agreement between the computed and measured flowfields.

The particular wing geometry of interest in this study is one with a ducted tip. A ducted tip geometry on a hydrofoil or propeller is one in which flow-through ducts, aligned approximately with the blade chord, are affixed at the blade tips. The ducted tip geometry was first proposed by Green et al. (1988). Water and wind tunnel tests of ducted tip hydrofoils have shown that the flow-through ducts suppress the tip vortex roll-up, thus resulting in a

¹ Department of Mechanical Engineering, University of British Columbia, 2324 Main Mall, Vancouver, BC, Canada.

substantial delay in the onset of tip vortex cavitation (Green and Duan, 1995). Also, sea trials of a ducted tip propeller have been conducted. A study on two 4 bladed, 36 inch diameter (29 inch pitch) propellers, one conventional and one fitted with ducted tips, has shown that the cavitation inception index for the ducted tip propeller is 50% lower than that for the conventional propeller. This comes *without* efficiency penalties. The efficiency of the ducted tip propeller is in fact up to 6% higher than the efficiency of the conventional propeller (Hordnes and Green, 1998).



Fig. 1 The Ducted Tip Propeller

In the previous studies mentioned above, the ducted tip has been selected in a fairly ad hoc way, without a detailed understanding of the three-dimensional aerodynamics around the duct. The aim of our study is to use a CFD model to optimize the shape and location of the ducted tip. The CFD model of the propeller is being made in several steps. First a 2D hydrofoil is modeled followed by a 3D hydrofoil with a rounded tip. These cases are validated with experimental data. Next a 3D hydrofoil with a ducted tip will be studied and eventually a 3D propeller with ducted tips will be considered. In this paper, computational results for 3D hydrofoils with round tips are presented and compared to experimental data.

NUMERICAL IMPLEMENTATION

The current study considers a steady flow past two hydrofoils with NACA 0012 and NACA 0015 airfoil sections. The hydrofoils, their computational domains, and the flow properties of the surrounding fluid have been chosen with comparison to available experimental data in mind. The NACA 0012 airfoil results are compared to the experimental results of Dacles-Mariani et al. (1995). The NACA 0015 airfoil results are compared to the experimental results of McAlister and Takahashi (1991). These different cases will be referred to as the Dacles-Mariani case and the McAlister case.

Geometry and Grid Generation

The NACA 0012 hydrofoil has an aspect ratio of 0.75 and the NACA 0015 hydrofoil has an aspect ratio of 3.3. Both aspect ratios are based on semispan and both hydrofoils have no twist or taper. The semispan is measured from the root of the foil to the quarter chord point on the round tip. The edge shape of the round tip of both foils is formed by rotating the two dimensional hydrofoil section around its camberline. Both foils are tilted around their quarter chord lines when run at an angle relative to the freestream flow.

Several grid generation methods have been explored in attempts to resolve the flow near the tip-vortex core and the hydrofoil surface. The multiblock grids that have been used for the study presented here consist of both structured hexahedral and semistructured prismatic blocks. The grids have been generated with CFD-GEOM from CFD Research Corporation. A C-mesh has been wrapped around a two dimensional section of the hydrofoil and extruded along the foil from the symmetry plane to the opposite side of the domain to form a C-H mesh.

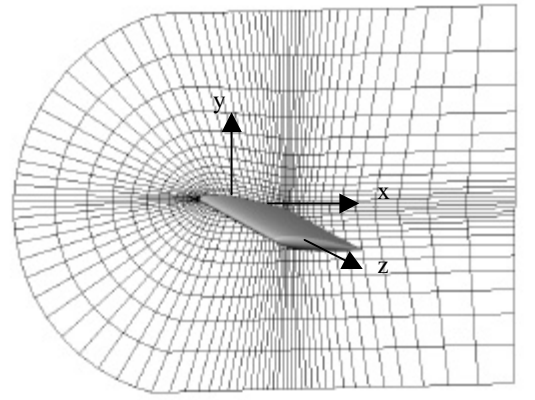


Fig. 2 The 2D C-mesh is extruded along the foil in the z-direction to the plane opposite to the tip of the hydrofoil

The cavity formed between the tip of the foil and the opposite wall has been filled with an H-H mesh extending approximately from 3% of the chordlength to 94% of the chordlength of the hydrofoil. The leading and trailing edge parts of the tip have been gridded with a triangular surface grid, which has then been extruded across the domain forming a prismatic grid to match the C-H and H-H blocks. To avoid very skewed cells at the leading edge and high aspect ratio cells at the trailing edge tip, these regions were meshed prismatically.

The dimensions of the computational domains for the McAlister case and Dacles-Mariani case are as follows.

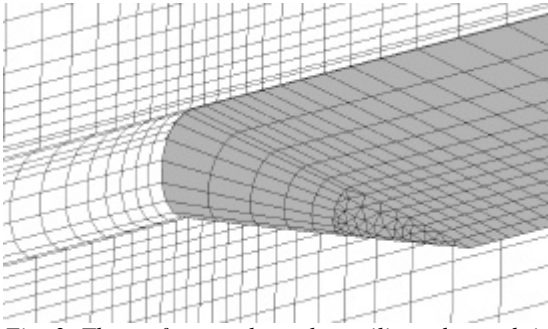


Fig. 3 The surface mesh on the trailing edge and tip of the hydrofoil and a cut of the grid in the x - z plane

McAlister Case. The 3.3 aspect ratio hydrofoil is placed with its quarter chord line 3.5 chord lengths from the top and bottom symmetry planes. The domain is 5 chordlengths wide (spanwise). The domain extends 2.5 chordlengths downstream of the trailing edge and 2 chordlengths upstream of the leading edge.

Dacles-Mariani Case. The 0.75 aspect ratio hydrofoil is placed with its quarterchord line 0.33 chord lengths from the top and bottom symmetry planes. The domain is 1 chordlength wide (spanwise). The domain extends 2 chord lengths downstream of the trailing edge and 2 chord lengths upstream of the leading edge. It should be noted that in order to provide an inlet sufficiently far upstream for the Dacles-Mariani domain, the front part of the C-H mesh (which only extended 0.3 chord lengths upstream from the leading edge) was matched with an H-H mesh to provide an inlet 2 chord lengths upstream of the leading edge.

Numerical Method

The pressure-based, finite-volume flow solver CFD-ACE(U) from CFDRC has been used in this study. The code uses unstructured/hybrid grids to integrate the Navier-Stokes equations. Cases have been run with a $k-\epsilon$ turbulence model and a second-order accurate upwind differencing scheme.

Boundary Conditions

Since each grid consists of multiple blocks, two types of boundary conditions have to be specified: 1) the physical boundaries such as inflow, outflow and walls and 2) the block-interface boundaries across which all flow quantities must be continuous.

For the physical boundaries, freestream velocity is specified for the inlet and constant

pressure for the outlet. Other sides, corresponding to the walls of the tunnel being modeled, are specified as symmetry walls. On the solid hydrofoil surface, a no-slip flow condition is used.

RESULTS

Given that the aim of this study is to provide a good base for modeling the flow around a ducted tip hydrofoil and later the ducted tip propeller, the focus in this study has primarily been on grid dependence and validation of the numerical results with experimental data.

Grid Dependence

Grid dependence has been studied for the McAlister case. The primary grid used for the McAlister case in this study has a total of approximately 436,000 cells. The C-H grid has $159 \times 35 \times 77$ grid points in the streamwise, surface-normal and spanwise directions, respectively. 101 of the 159 streamwise grid points and 43 of the 77 spanwise grid points are used on the hydrofoil. The first grid spacing on the hydrofoil surface is specified at 0.001 chord length above the hydrofoil surface. The H-H grid extending from the midsection of the tip has $29 \times 17 \times 35$ grid points and the nose and tail prism grids have 8092 and 4216 cells respectively.

The results obtained from the primary grid are compared with the results obtained from a 153,000 cell grid in Figure 4 and 5. The main difference in the two grids lies in the first cell spacing (0.004 chordlength in the less dense grid) and a less resolved tip vortex both in the streamwise and spanwise directions. Figure 4 shows the surface pressure distribution close to the midspan of the hydrofoil obtained from the different grids. The dense grid causes negligible difference in the pressure on the pressure side on the hydrofoil. The primary difference can be seen in the pressure peak on the suction surface. The difference can be attributed to a better resolved mesh at the leading edge for the grid with more cells. Close to the tip there is more difference in the pressure distribution obtained from the two grids as is shown in Figure 5. As can be seen there is little difference in the pressure on the pressure side but a significant difference on the suction side, especially towards the trailing edge where the tip vortex starts to roll up. It is expected, and shown here, that greater resolution of the leading edge and the tip vortex region causes higher pressure peaks to be predicted.

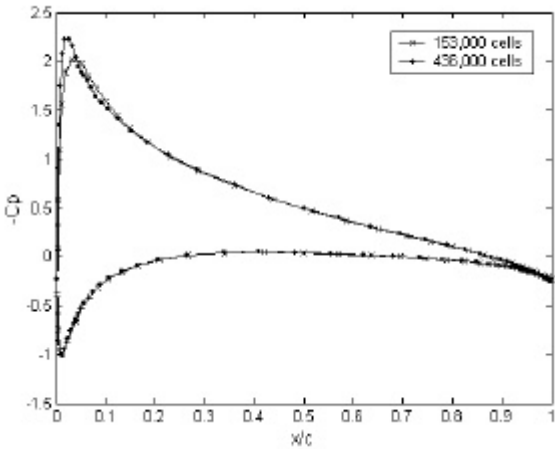


Fig. 4 Comparison of the chordwise pressure distribution at $z/s = 0.55$ for different density grids

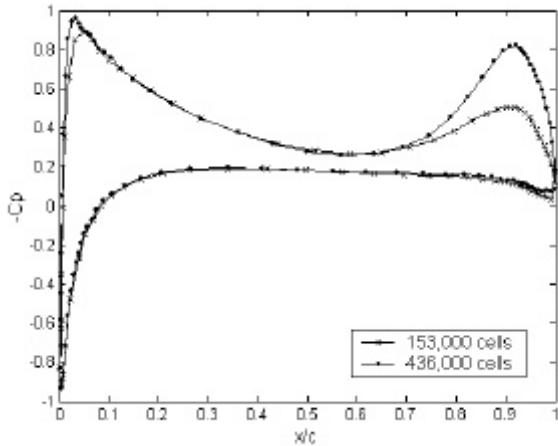


Fig. 5 Comparison of the chordwise pressure distribution at $z/s = 0.971$ for different density grids

Comparison with the experimental results of McAlister and Takahashi (1991)

The primary computation conducted for comparison with McAlister's and Takahashi's data was done at Reynolds number $Re = 2.9 \times 10^6$ (based on the chordlength and the free stream velocity) and angle of attack $\alpha = 8$ degrees. Figures 6 and 7 show the surface pressure distribution at two different spanwise stations, away from and close to the tip. Away from the tip the agreement is generally quite good. The computed suction side pressure coefficient is slightly lower than McAlister and Takahashi's experimental data. It is likely that a greater number of grid points in the leading edge region will produce a better resolved suction peak. Close to the tip the agreement is worse. The pressure distribution towards the tip is determined by the

details of the three dimensional tip vortex rollup and separation from the surface. It is likely that a combination of poor grid resolution and a low order accuracy scheme along with diffusion in the turbulence model cause the strength of the vortex to be underpredicted. The agreement with experiments is generally good away from the tip and poorer close to the tip, which is consistent with the findings of Hsiao and Pauley (1998).

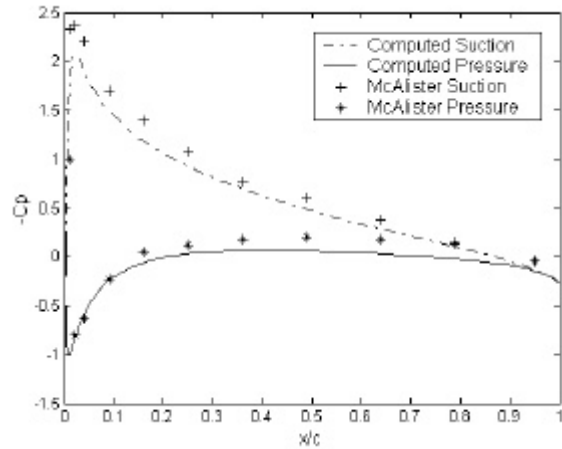


Fig. 6 The chordwise pressure distribution on the hydrofoil surface at $z/s = 0.676$ (measured from root of foil) for $\alpha = 8$ degrees and $Re = 2.9 \times 10^6$

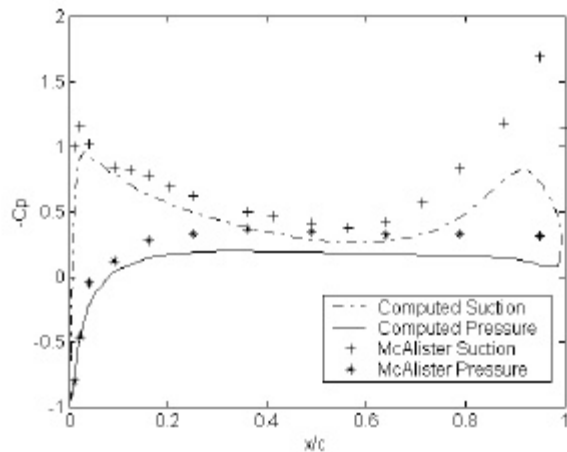


Fig. 7 The chordwise pressure distribution on the hydrofoil surface at $z/s = 0.971$

The pressure-derived lift distribution over the outer portion of the wing was computed and is compared to experimental data in Figure 8. Close to the tip the difference in experimental and computational lift coefficients is up to 0.07 whereas further away from the tip the difference is around 0.01-0.015. The computed total lift coefficient is 0.66, which compares well to a lift coefficient of 0.67

predicted by lifting line theory for a wing of the same aspect ratio.

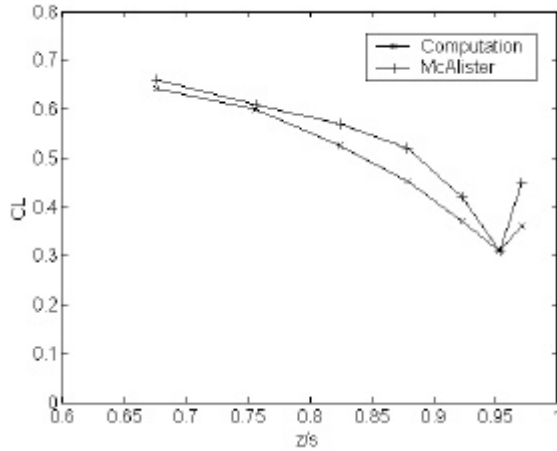


Fig. 8 Pressure derived lift distribution over outer portion of wing

Comparison with the experimental results of Dacles-Mariani et al. (1995)

The primary computation conducted for comparison with the experimental data of Dacles-Mariani et al. was done at Reynolds number $Re = 4.6 \times 10^6$ (based on the chordlength and the free stream velocity) and angle of attack $\alpha = 10$ degrees. The grid has around 205,000 cells with the first grid cell located at 0.0012 chord lengths above the hydrofoil surface. The C-H mesh has 145x25x51 grid points in the streamwise, surface-normal and spanwise directions, respectively. 97 of the 145 streamwise grid points and 32 of the 51 spanwise grid points are used on the hydrofoil. The inlet H-H mesh has 15x31x51 grid points and the H-H mesh along the tip of the foil has 30x15x20 grid points. The nose and tail prismatic grids have 2812 and 3040 cells respectively.

Presented in Figure 9 is a comparison of the computed and experimental pressure distribution along the hydrofoil surface close to the tip (located roughly under the vortex). Although there are some differences, the plot indicates that the vortex-induced peak suction is captured reasonably well by this computation. Figure 10 shows the total velocity magnitude across the vortex core about a quarter chord behind the trailing edge. The agreement between the experimental and computed shapes of the velocity magnitude distribution indicates that the spanwise location of the vortex is predicted correctly. However, unlike the experimental measurements, the velocity does not reach a peak in the middle of the vortex core, but instead dips. The dip in the total

velocity magnitude is likely caused by a combination of poor grid resolution around the vortex core and diffusion of the vortex by the turbulence model. Dacles-Mariani et al. observed a similar dip in the total velocity, even though they used a 5th order accurate upwind-biased differencing of the convective terms and a Baldwin-Barth turbulence model. Their results are shown in Figure 10 as well. By modifying the production term in the model to suppress excessive diffusion of the vortex they were able to predict the velocity peak closer to the experimentally measured velocity peak (Dacles-Mariani et al., 1995). It should be noted that for the computation of the velocity magnitude in the vortex core, Dacles-Mariani et al. set computational flow conditions at the trailing edge to match experimental data.

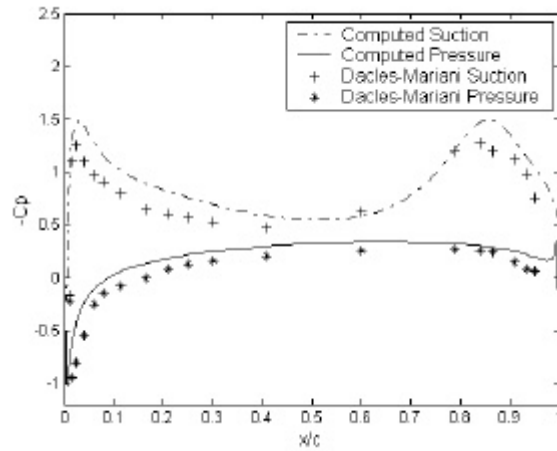


Fig. 9 The chordwise pressure distribution on the hydrofoil surface at $y/z = 0.667$ ($y/s = 0.89$)

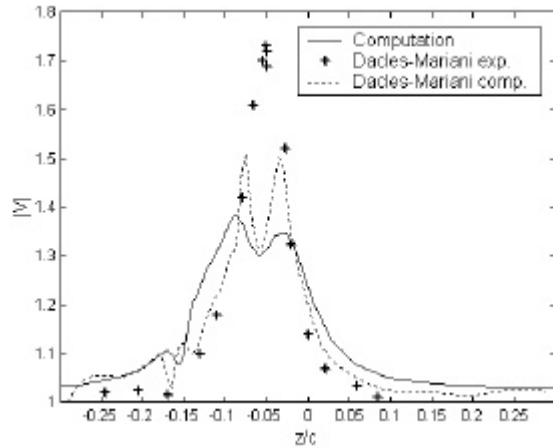


Figure 10 Total velocity magnitude across vortex core at $x/c = 0.24$ aft of the trailing edge.

CONCLUSIONS

The flow over a finite-span hydrofoil has been studied using the finite-volume flow solver CFD-ACE(U) from CFDRC. A K- ϵ turbulence model and a combination of C-H, H-H and prism grids were used. Cases were run with a second order accurate upwind differencing scheme and the results compared to available experimental data. The aim of the study was to provide a good basis for future modeling of ducted tip hydrofoils and a ducted tip propeller.

Key results from this study include the following:

1. Grid convergence studies have shown that an increase in number of cells is unlikely to cause a great difference in the pressure distribution along the hydrofoil away from the tip but will likely increase suction peaks significantly close to the hydrofoil tip.
2. Comparison with the experimental results of McAlister and Takahashi shows that more than 0.2 spanwidths away from the tip, sectional lift is predicted within 2% of the experimental data whereas closer to the tip the difference reaches up to 12%. The total lift is in good agreement with lifting line theory. The discrepancy in pressure distribution close to the tip can likely be attributed to poor grid resolution, diffusion in the turbulence model and a low order differencing scheme.
3. Comparison with the experimental results of Dacles-Mariani et al. shows good prediction of the spanwise location of the vortex core and indicates that the vortex induced pressure peak is captured reasonably well.

Future work will include developing a Pro Engineer model of a hydrofoil with a ducted tip and running simulations for the flow around it. Particular interest in future simulations is the overall performance of the hydrofoil, which is largely indicated by the overall lift coefficients, that have been shown here to be well predicted. A final stage of the research will involve simulation and optimization of ducted tip propellers.

REFERENCES

Crump, S. F., 1948, "The Effects of Bulbous Blade Tips on the Development of Tip Vortex Cavitation on Model Marine Propellers," report C-99, David Taylor Naval Ship Research and Development Center.

Dacles-Mariani, J., Zilliac G. G., Chow, J. S. and Bradshaw, P., 1995, "Numerical/Experimental Study of a Wingtip Vortex in the Near Field," AIAA Journal, Vol. 33, No. 9, pp. 1561-1568.

Green S. I. and Duan S. Z., 1995, "The Ducted Tip – A Hydrofoil Tip Geometry with Superior Cavitation Performance," ASME Journal of Fluids Engineering, Vol. 117, pp. 665–672.

Hordnes, I. and Green S. I., 1998, "Sea Trials of the Ducted Tip Propeller," ASME Journal of Fluids Engineering, Vol. 120, pp. 808–817.

Hsiao, C. and Pauley, L. L., 1998, "Numerical Study of the Steady-State Tip Vortex Flow Over a Finite-Span Hydrofoil," ASME Journal of Fluids Engineering, Vol. 120, pp. 345-353.

Itoh, S., 1987, "Study of the Propeller with Small Blades on the Blade Tips (2nd Report: Cavitation Characteristics)," Journal of the Society of Naval Architects of Japan, Vol. 161, pp. 82-91. Published in Japanese with English abstract.

Mani, K., Sharma, S. D., and Arakeri, V. H., 1988, "Effect on Propeller Blade Modification on Cavitation Induced Noise," ASME FED, Vol 64, pp. 64-67.

McAlister, K. W., and Takahashi, R. K., 1991, "NACA 0015 Wing Pressure and Trailing Vortex Measurements," NASA Technical Paper 3151.

www.cfdrc.com

